PNAS RESEARCH ARTICLE | ENVIRONMENTAL SCIENCES
SUSTAINABILITY SCIENCE

# Warming climate and water withdrawals threaten river flow connectivity in China

Jiaojiao Gou[a,b], Chiyuan Miao[a,1], Jinren Ni[c], Soroosh Sorooshian[d], Qingyun Duan[e], Denghua Yan[f], Louise Slater[g], Zongxue Xu[h,i], Alistair G. L. Borthwick[j,k], Lu Su[l], Qi Zhang[a], and Yoshihide Wada[m]

Affiliations are included on p. 10.

Edited by Andrea Rinaldo, Ecole Polytechnique Federale de Lausanne, Lausanne, Switzerland; received October 14, 2024; accepted July 8, 2025

**River flow connectivity, the continuity of fluvial discharge in space and time, provides a crucial lifeline for most biotic communities on Earth. Yet there is still limited understanding of the impacts of climate change and human water withdrawal on river connectivity. Here, we assess the river flow connectivity of 217,001 river reaches in mainland China from 1961 to 2020 and the impact of different climate warming trends and water withdrawals for different sectors. We estimate that naturally intermittent rivers represent about 13% of all river reaches, with a large contrast between northern and southern China (12% vs. 1%, respectively). Although river intermittency decreased slightly during this period (i.e., river connectivity lengthened due to increasing precipitation), warming temperatures offset this decrease by reducing surface water persistence, causing the decrease (−476 vs. −233 km/y) to double when removing the long-term temperature trend. Critically, the length of intermittent rivers increased remarkably from 13 to 50% when considering human water withdrawal by agricultural, domestic, and industrial sectors, in addition to environmental flow requirements. Our findings highlight the urgent need to maintain sustainable water resources in a warming climate in which unregulated water abstractions increasingly threaten river flow connectivity, particularly in drying regions.**

hydrology | river connectivity | water withdrawals | climate change | China

## Significance

River flow connectivity is vital for sustaining freshwater ecosystems, which are essential to life on Earth. Although the warming climate and increased human water abstraction pose significant threats to this connectivity, their impacts remain poorly understood. Our study estimates that about 13% of all river reaches in mainland China are natural intermittent rivers. Despite slight increases in river connectivity during 1961–2020, climate warming has offset these gains by reducing surface water persistence. Human water withdrawals have also greatly impacted river functional connectivity, with the number of intermittent rivers rising from 13 to 50% to meet growing water demands. Understanding the drivers behind these changes is crucial for preserving the ecological and functional integrity of river systems in the future.

Rivers provide fresh water, food, transportation corridors, and energy for life on Earth (1). The sustainable provision of water plays a pivotal role in ecosystem sustainability (2), regional socioeconomic development (3), and human well-being (4). River flow connectivity defines the flow status and carrying capacity of a river and is associated with a range of important ecological and societal benefits (5–7). A surprisingly large proportion, about 51 to 60%, of the world's river water ceases to flow for at least one day per year, demonstrating the roughly equal importance of intermittent and perennial rivers in maintaining the functional integrity of fluvial systems (6, 8). However, the spatial extent of and temporal changes in river connectivity are largely unknown. In China, connectivity has only been examined for individual basins, (9, 10) and there is a lack of information on the numbers of intermittent rivers flowing through different hydroclimatic zones.

Gauged streamflow monitoring (11, 12) and recently machine learning (6) techniques have been used to estimate the proportion and distribution of intermittent rivers and explore their drivers. However, the distribution of intermittent rivers is hard to estimate from observed streamflow records because gauging stations are preferentially installed along perennial rivers (13), which very likely omit the effect of smaller channels (14). Moreover, streamflow data are scarce for arid regions, and error inevitably arises from inadequate measurement techniques and/or gauge maintenance (15, 16). In contrast, machine learning provides a probabilistic prediction technique for spatially continuous river hydrography, but its effectiveness is challenged by the unequal distribution of available training data, particularly in China (only 25 gauged stations were used in ref. 6).

Natural river flow connectivity is highly sensitive to changes in aridity (5, 6, 8, 12), which is vulnerable even to small changes in climate, especially during prolonged droughts. Given the increase in global mean temperature over the past hundred years (17), interest is also growing in the changing behavior of river flow connectivity as the environment warms (5, 18, 19). Although many studies have evaluated the association between streamflow signatures and different climate variables (6, 12) (such as aridity index, temperature, precipitation, and evapotranspiration), few have assessed the combined effects of temperature and precipitation trends on river flow connectivity at different warming levels. Moreover, increased human water withdrawal alongside socioeconomic development can threaten the health of riverine ecosystems (20, 21). For example, a perennial river might

Author contributions: J.G., C.M., and J.N. designed research; J.G., C.M., L. Slater, and Y.W. performed research; J.G., C.M., J.N., S.S., Q.D., D.Y., L. Slater, Z.X., A.G.L.B., L. Su, Q.Z., and Y.W. contributed new reagents/analytic tools; J.G., C.M., J.N., S.S., Q.D., D.Y., L. Slater, Z.X., A.G.L.B., L. Su, and Q.Z. analyzed data; and J.G., C.M., A.G.L.B., and Y.W. wrote the paper.

The authors declare no competing interest.

This article is a PNAS Direct Submission.



[1]To whom correspondence may be addressed. Email: miaocy@bnu.edu.cn.

This article contains supporting information online at https://www.pnas.org/lookup/suppl/doi:10.1073/pnas.2421046122/-/DCSupplemental.

Published August 18, 2025.

transition to intermittent when water consumption for agricultural irrigation increases. Sustainable rivers should meet the needs of increasing human water demand and eco-environmental sustainability without compromising the connectivity of the riverine system or damaging fundamental processes and their functionality.

To date, the effects of warming climate and human water abstraction on the spatial-temporal variation of river flow connectivity have yet to be fully investigated. We propose a unique approach to quantify river flow functional connectivity focusing on the example of Chinese rivers. As the fastest growing country and the world's second-largest economy, China has experienced a doubling of water consumption from 1965 to 2013 (22). Previous global nonperennial river assessments (1, 6) have played a critical part in riverine system protection efforts, but there is a lack of sufficiently fine-resolution or high-quality bias-corrected natural flow data for China.

Here, we analyze the spatial and temporal patterns of natural river flow connectivity in mainland China during 1961–2020, using daily natural streamflow simulation for 217,001 mapped river hydrography survey locations, obtained using a calibrated land surface model (15, 23) coupled with a river routing model, called the Routing Application for Parallel Computation of Discharge (RAPID) (*SI Appendix*, Fig. S1). We develop an automatic statistical postprocessing procedure, Upstream-Downstream Scaled Bias Correction (UDSBC), to reduce model simulation bias for each river reach. Based on reconstructed high-quality daily streamflow and historical climate change signals, we then use three temporal and one spatial streamflow signature to quantify the spatial-temporal dynamics of river flow connectivity and analyze the climate impact mechanism for intermittent rivers across China. A historical human water withdrawal dataset is used to estimate natural river carrying capacity and hence assess whether a given river can meet water consumption and environmental flow requirements for agricultural, domestic, and industrial sectors, in addition to ecological services. We propose a unique approach to quantify river flow functional connectivity and identify the shortfall in surface water when the supply in a given month fails to meet the corresponding average human water demand. The *Materials and Methods* provides definitions of the terms, natural streamflow, river flow connectivity, and river flow functional connectivity, used herein.

## Results

**Detected Decrease in Natural River Intermittency Across China.** We first examine the spatial and temporal patterns of natural river connectivity in mainland China in recent decades by considering the reconstructed natural streamflow of 217,001 river reaches across China (Fig. 1*A*). Of these river reaches, 13% met the criteria for natural flow intermittence throughout the 1961–2020 period with recorded lengths of natural intermittent rivers ranging from 0.06 to 108.14 km (Fig. 1*B*). Moreover, our analysis reveals large spatial variation in river flow connectivity, in line with the high variability of surface water frequency of occurrence across China (2). The majority of intermittent rivers are located in northern basins, whereas perennial rivers are located in the southern basins (Fig. 1*B*). Across the ten large river basins (*SI Appendix*, Table S1), the Northwest River drainage system exhibits the highest proportion (12% of all rivers) of intermittent rivers, with $2.2 \times 10^5$ km of river reaches experiencing at least one zero-flow day per year (Fig. 1*C* and *SI Appendix*, Fig. S2). The Southeast River drainage system has the lowest recorded length of intermittent rivers (120 km, Fig. 1*C* and *SI Appendix*, Fig. S2). The spatial distribution of intermittent rivers can be attributed to climate conditions, in particular aridity, which is a leading factor in river streamflow intermittency (6, 12). Generally speaking, the water occurrence rate is higher in the humid river basins than in the arid northwestern regions, where evaporation rates considerably exceed precipitation for at least part of the year. We also found that flow intermittence usually occurs in low-order rivers (Strahler stream order 1 to 2, accounting for 93% of all rivers) and attenuates with increasing channel order (Fig. 1*C*). This reflects a possible deficiency arising from the use of gauge observations to assess river flow connectivity, because gauging stations are preferentially installed on perennial (high-order) rivers whereas flow intermittence is more likely to occur in low-order rivers.

Linear trend analysis reveals that the length of natural intermittent rivers exhibits an insignificant decreasing rate of −233 km/y ($P > 0.1$) during 1961 to 2020, indicating that decreasing river intermittency is prevalent across China during this period, despite substantial year-to-year variability (Fig. 1*D*). This decline trend is closely linked to the spatial patterns of the annual rates of change in precipitation and discharge, whereby a larger proportion of river reaches have experienced increasing precipitation and discharge over recent decades (*SI Appendix*, Figs. S3 and S4). Specifically, rivers with significant decreasing intermittency are primarily located in the northwestern region, owing to the reduced occurrence of zero-flow days following from the decreased frequency of short-duration, stream dry-out events (*SI Appendix*, Fig. S2 *D*–*F*). The results also reveal a large increase in river intermittency in 6.2% of the total river length, mainly located in the northern Inner Mongolia region (*SI Appendix*, Fig. S2). Overall, the change trend toward river intermittency is most likely driven by climatic conditions (6, 12) (*SI Appendix*, Figs. S3 and S4). To further test the robustness of our results, we performed sensitivity assessments on the zero-flow threshold (ranging from 0.0001 to 0.01 $m^3$/s) and cessation length (ranging from 1 to 30 d), which provided insight into the land surface model uncertainty. The trend change in river flow intermittency is generally consistent under the different thresholds (*SI Appendix*, Table S2), indicating that threshold selection influences the estimated change rate in intermittent river length, whereas the overall direction of change—toward decreasing intermittency—is consistent regardless of threshold.

The spatial connectivity of river flow, as measured by a revised dendritic connectivity index (DCI) (5, 24), also exhibits significant spatial and temporal variability across the ten river basins of China. The DCI ranges from 0 to 100% and quantifies the degree and duration by which a given river network is connected to or disconnected from a river basin in terms of the combined length of zero-flow reach fragments (*Materials and Methods*). Large river basins with highly nested river networks such as the Yangtze and Yellow river basins tend to exhibit high spatial connectivity (mean DCI > 80%; Fig. 2 *E* and *F*). Conversely, lower DCI values (below 20%) generally occur in flat or dry basins, such as the Hai river basin and the Northwest River drainage system with an average elevation of 597 m and an annual precipitation below 200 mm, respectively (Fig. 2 and *SI Appendix*, Table S1), indicating a more fragmented river network. The DCI follows a seasonal climate cycle that exerts strong influence on spatial connectivity throughout the river network (Fig. 2). Connectivity naturally declines during the dry season (November-April) in most river basins as precipitation decreases and intermittent stream channels dry out (Fig. 2). In the summer monsoon season, the river network experiences long episodes during which wetted areas tend to expand.

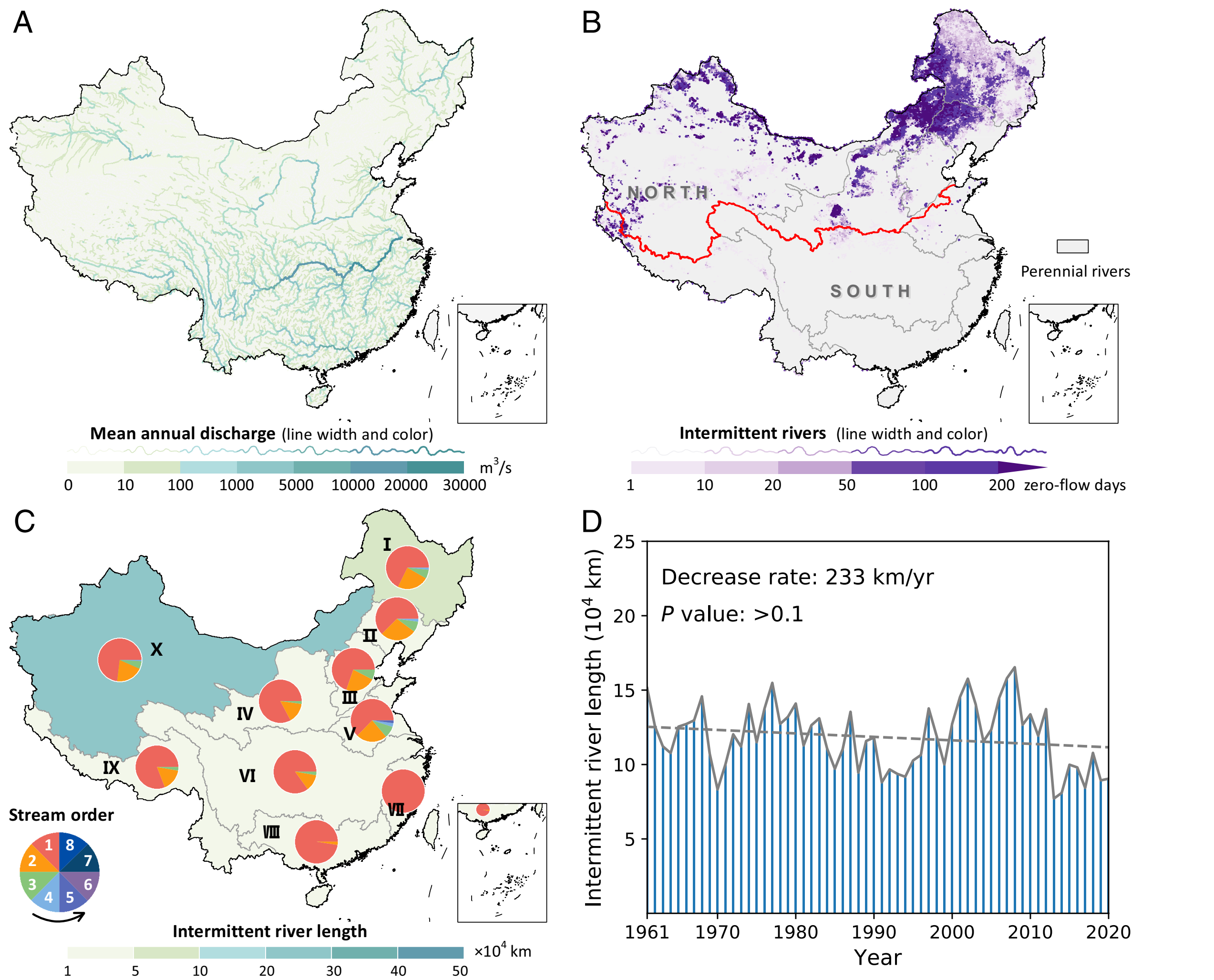


**Fig. 1.** Distribution of and changes in natural intermittent rivers during 1961–2020 across China. (*A*) Spatial distribution of mean annual natural river discharge (streamflow, m$^3$/s) for 217,001 river reaches across China. (*B*) Spatial distribution of intermittent rivers, defined as at least one zero-flow day per year on average, throughout the national river and stream network. (*C*) Spatial distribution of intermittent river lengths for the ten large river basins in China: I, Songhua River; II, Liao River; III, Hai River; IV, Yellow River; V, Huai River; VI, Yangtze River; VII, Southeast River drainage system; VIII, Pearl River; IX, Southwest River drainage system; and X, Northwest River drainage system. Pie charts show distributions of intermittent river length in eight Strahler stream orders. (*D*) Trend in annual intermittent river length across China. The dashed gray line indicates the linear trend line during 1961–2020.

Seasonal patterns are more obvious in semiwet and semidry river basins where channels are prone to water constraints, such as in the Songhua river basin (Fig. 2*A*) and Yellow river basin (Fig. 2*E*). In humid environment such as in the Southeast River drainage system and the Pearl River basin, where rainfall and river flow are high throughout the year, the seasonal patterns of spatial connectivity can be diminished by the steady water supply (Fig. 2 *G* and *H*). Intra-annual variability of daily DCI is higher in semiwet and semidry river basins (including the Songhua River, Liao River, Huai River, and Yellow River) than in very wet and very dry river basins, confirming that water seasonal variations are larger in semiwet and semidry river basins, and are more strongly associated with spatial connectivity than in dry and wet river basins. Consistent with the widespread lengthened river connectivity (*SI Appendix*, Fig. S2), most of the ten large river basins exhibited insignificant increasing spatial connectivity (*SI Appendix*, Fig. S5). By contrast, the spatial connectivity of the river networks displayed insignificant declining trends in the Yellow River basin and Liao River basin. These spatial connectivity results provide additional support for the conclusion that river intermittency has decreased widely across China from 1961 to 2020 (Fig. 1*D*).

**Offsetting Effect of Warming on the Decrease in Intermittent River Length.** To examine whether the detected decreases in river intermittency were offset by long-term warming (25) (*SI Appendix*, Figs. S3*D* and S4), we detrended the climate forcing using a linear fit and then repeated simulations S2 and S3 (*Materials and Methods*). Our results show that the declining trends in intermittent river length for the temperature-detrended simulation (−476 km/y) are more than double for the raw simulation (−233 km/y, Fig. 3). Furthermore, the trend for intermittent rivers tends to increase with the warming impact alone compares to the raw simulation (177 km/y vs. -233 km/y, Fig. 3). The warming climate appears to have offset the decrease in intermittent river length and caused the intermittent river networks to expand. In other words, without the drying effect of climate warming, river connectivity would have increased further due to the wetting trend, indicating that the decreasing trend was slightly offset by the long-term temperature trend.

To further investigate the climate-change impact mechanism on river-flow connectivity, we examined historical trends in the streamflow signatures of rivers located in six distinct climatic regions. The T and P subscripts indicate temperature

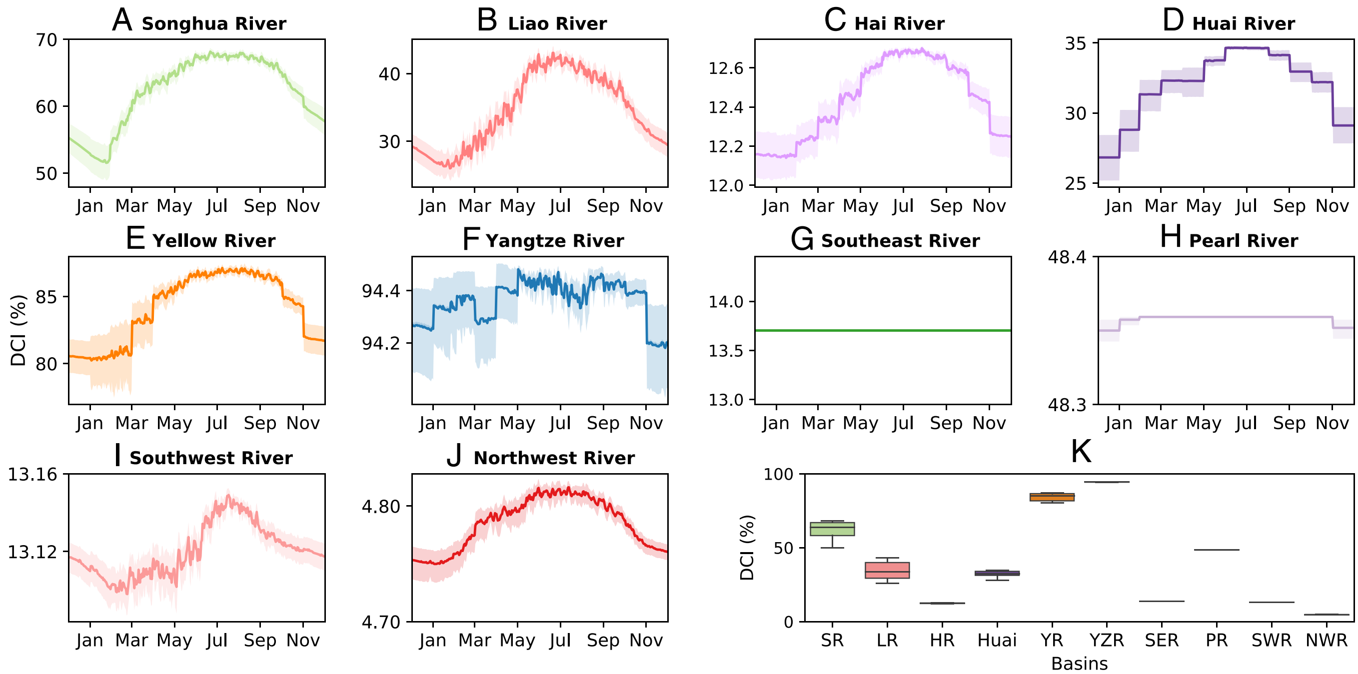


**Fig. 2.** Spatial connectivity in the ten large river basins in China. (*A–J*) Mean daily dendritic connectivity index (DCI, %) during 1961–2020 for the Songhua River (SR), Liao River (LR), Hai River (HR), Huai River (Huai), Yellow River (YR), Yangtze River (YZR), Southeast River drainage system (SER), Pearl River (PR), Southwest River drainage system (SWR), and Northwest River drainage system (NWR). Solid lines show mean daily DCI, with the colors indicating each large river basin. The shaded area represents the Student's *t* 95% CI of mean daily DCI values for each large river basin. (*K*) Intra-annual variability of daily DCI values obtained for each large river basin. Here, intra-annual variability is measured using the multiyear mean DCI for each day of the year.



and precipitation change levels; for example, $T_LP_+$ refers to river reaches with low warming and significant wetting trends. We find that the intermittent rivers under warming-wetting trends, characterized by a relatively consistent increasing water supply, generally exhibit a decreasing trend (Fig. 4*A* and *SI Appendix*, Fig. S6). From the warming magnitude perspective, we find that rivers in the low warming region ($T_LP_+$) present the strongest decreasing trend in mean zero-flow days with −6 d/10 y, whereas rivers in $T_MP_+$ and $T_HP_+$ present more moderate decreasing trends of −4 d/10 y and −6 d/10 y, respectively (Fig. 4*A*). The results indicate that warming imposed an offsetting effect on the historical decrease in intermittent river length in regions experiencing warming-wetting trends. In other words, climate warming has increased the probability of occurrence of nonperennial flow regimes by reducing surface water persistence, as also observed in other regions (8). We note that the offsetting effect on the decrease in river flow intermittency did not grow steadily with increasing levels of warming. Meanwhile, the zero-flow period duration in $T_HP_+$ regions also decreased substantially, while the frequency of zero-flow periods exhibited an offset with the increasing number of river intermittent events (Fig. 4*A*). A possible explanation for this trend reversion with high warming is that a higher rate of temperature increase (> +0.4 °C/10 y) induced earlier snow melting, thus increasing transient water flux in clod seasons (26), resulting in short intermittent events that coalesced into longer duration intermittent events, which in turn increased the number of zero-flow days.

To assess the seasonal variability of our results, we also evaluated the trends in streamflow signatures for warming-wetting and warming-drying regions in wet and dry seasons (Fig. 4 *B* and *C*). Despite the similarity in the patterns of change for both wet and dry seasons, the absolute trend in zero-flow days was greater in the dry season than in the wet season, indicating that the rivers are more vulnerable to intermittency in dry seasons. The spatial connectivity of the Northwest River drainage system would be expected to increase in a warming-wetting climate because of decreased prevalence of intermittent rivers and including of a certain number of high-order rivers (*SI Appendix*, Fig. S7). Vulnerability in dry seasons may have been driven by increased evaporation, reducing available water (27), and by streams in dry seasons being more prone to intermittency owing to seasonal patterns of freezing, thawing, and/or drying (6).

Our results illustrate the diverse impact of climate change trends on river flow connectivity for the six grouped climate change region. Overall, warming-wetting climate change caused river flow connectivity to increase, with lower impact in areas with greater warming, and vice versa. These results indicate a possible offsetting effect of warming on the decrease in river intermittency, which means that future warming, particularly in dry regions, is likely to increase the risk of river channels drying out (without taking into account snowmelt recharge), especially in low-order rivers. Continued warming is likely to further reduce flows while increasing mean precipitation (28), which would be offset during periods of prolonged drought. Our findings align with those from other regions which imply warming (in the absence of significant wetting) leads to less river connectivity, such as in the Western United States (29).

**Human Water Withdrawal Threatens Natural Water Resource Sustainability.** Above-daily-flow connectivity analysis was first analyzed using natural streamflow data without human interference. Hence, we were able to investigate how human water withdrawal activities affected the ability of rivers to meet environmental streamflow requirements (*Materials and Methods*). Fig. 5 *A–C* displays the spatial patterns of mean annual zero-flow months obtained when accounting for the environmental streamflow and the water withdrawal volumes in agricultural, domestic, and industrial sectors. We found that loss of river flow functional connectivity was most serious in the agricultural sector, where $8.5 \times 10^5$ km of river reaches experienced at least

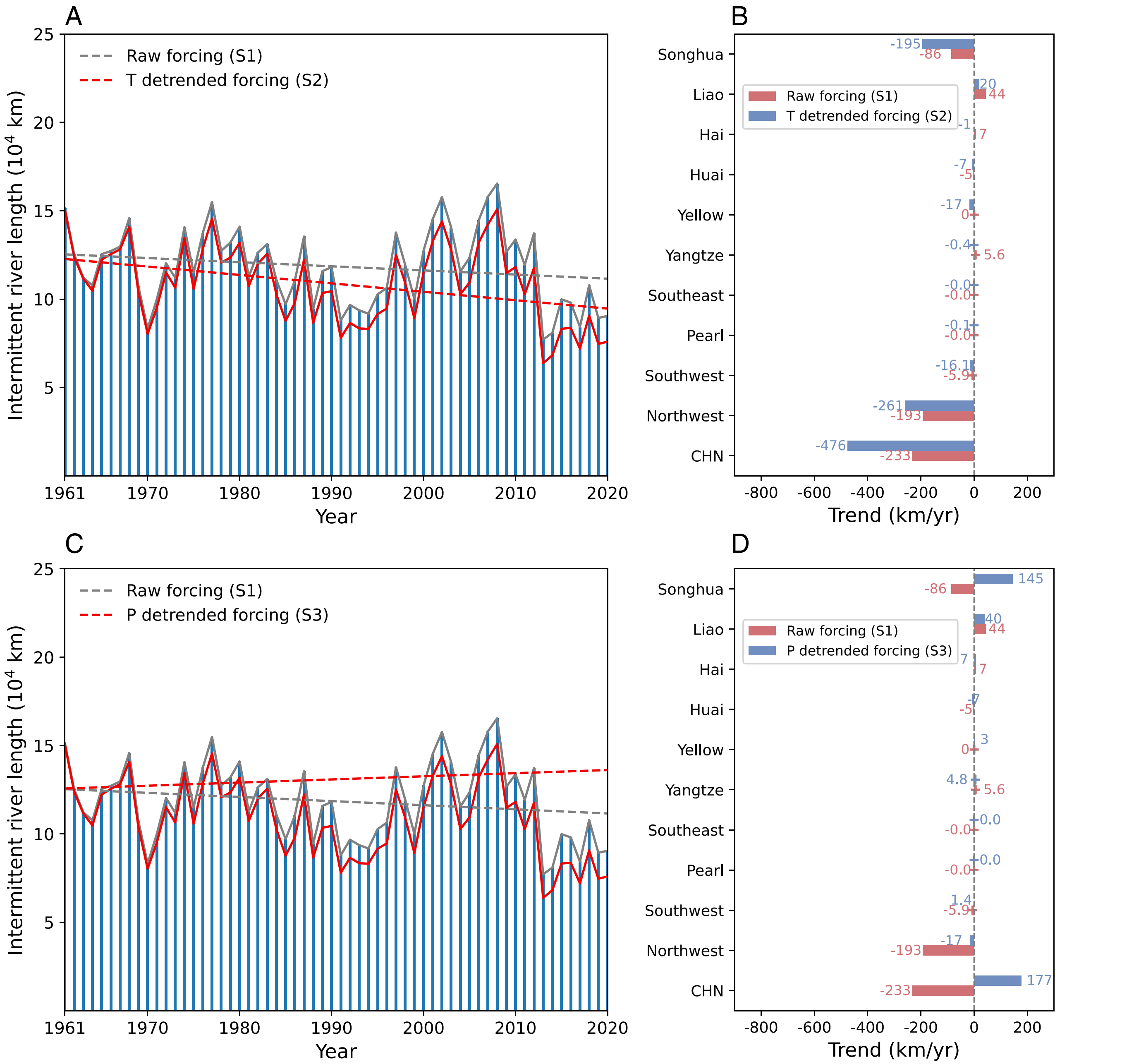


**Fig. 3.** Natural river flow connectivity changes with time for different climate-change scenarios. *A* and *B* show time series of intermittent river length corresponding linear trends across major basins and the whole region for raw forcing simulation (S1) vs. T-detrended forcing simulation (S2). *C* and *D* show time series of intermittent river length corresponding linear trends across major basins and the whole region for raw forcing simulation (S1) vs. P-detrended forcing simulation (S3). In *A* and *C*, the gray and red dashed lines indicate linear trends for raw forcing simulation and detrended forcing simulations. In (*B*) and (*D*), red and blue bars indicate linear trends for raw forcing simulation and detrended forcing simulations. Red and blue crosses on the zero-trend axis mark corresponding trend values for the Yangtze Southeast, Pearl, and Southwest River drainage systems (because the values for these basins are too small for the bars to be displayed properly). The numbers refer to the river length change trend for each simulation scenario.

one zero-flow month per year, corresponding to 46% of all river reaches and an average of three months of ineffective connectivity (Fig. 5). Water withdrawals by the industrial and domestic sectors resulted in 25 and 37%, respectively, of all river reaches ceasing to provide societal, economic, and ecological services for at least one month per annum. This result is reasonable given that agriculture, especially irrigation, is one of the largest water-use sectors in China (20, 22). Consequently, the proportion of intermittent rivers more than tripled from 13 to 50% when considering total human water withdrawals and environmental flow requirements, implying that human water withdrawals greatly threaten the sustainability of natural water resources in China. Accounting for return flow that replenished river flow, the proportion of functional intermittent rivers dropped from 50 to 43%, and further to 36% when excluding groundwater withdrawal in the evaluation of river flow functional connectivity (*SI Appendix*, Fig. S8). Even after considering compensation from groundwater and return flow, the proportion of functional intermittent rivers remained about three times higher than that of natural intermittent rivers (36% vs. 13%). The northern regions, notably the North China Plain and Northeast China Plain, experience severe loss of river flow functional connectivity, whereas the southern regions have higher capacity to support socioeconomic development, the environment, and aquatic ecosystem sustainability (Fig. 5 *A*–*C*).

The total length of intermittent rivers across all sectors (Fig. 5*D*), including agricultural, domestic, and industrial sectors, exhibits

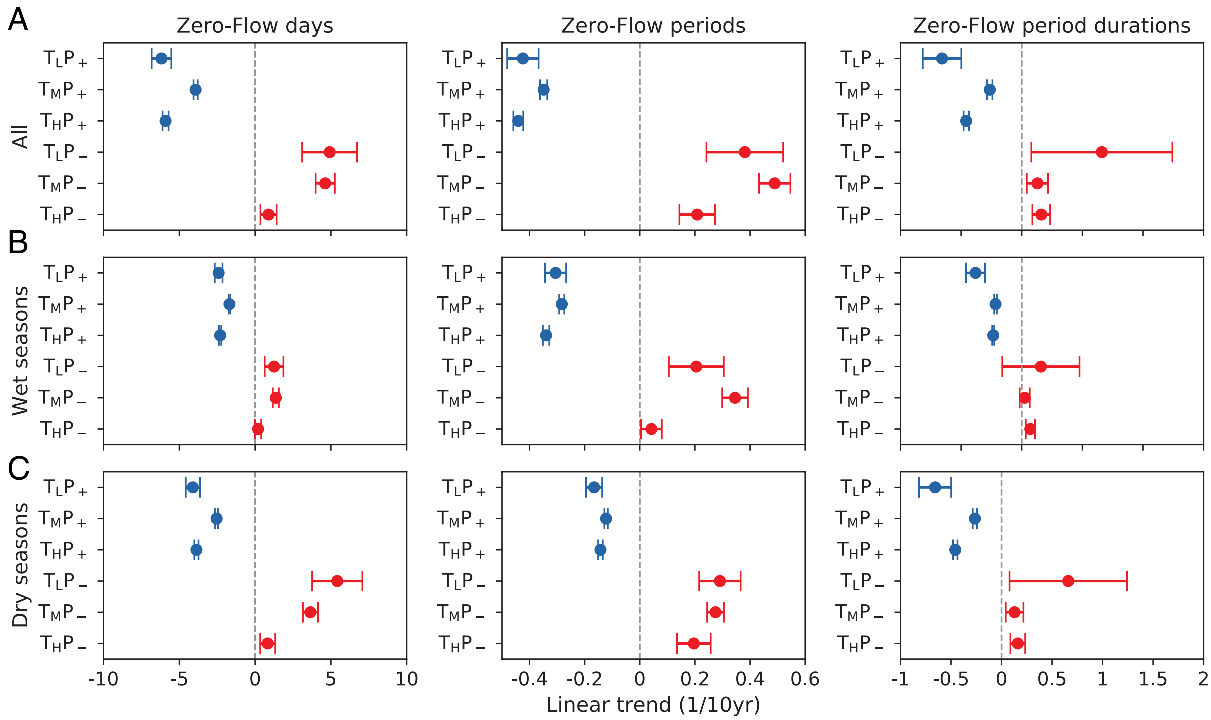


**Fig. 4.** Linear trend in three streamflow signatures during 1961–2020 in areas with warming-wetting and warming-drying climate trends, based on the mean annual number of zero-flow days, number of zero-flow periods, and duration of zero-flow periods (1 unit per 10 y) for three different timescales: (*A*) whole year, (*B*) wet seasons (May–October), and (*C*) dry seasons (November–April). Error bars represent the 95% CI of the mean trend. Blue bars denote regions with warming-wetting trends, and red bars denote regions with warm-dry climate regimes. Temperature subscripts, H, M, and L, represent high, moderate, and low warming levels. Precipitation subscripts, + and – signs indicate significant ($P < 0.05$) increasing and decreasing precipitation according to the Mann–Kendall test. For example, $T_LP_+$ refers to river reaches with low warming and significant wetting trends.

a decreasing trend of −3,461 km/y during 1961–2020. Of the three sectors, both industrial and domestic intermittent river lengths underwent rapid decline until just before 1972 and subsequently increased, reaching a steady state in 2010, after which they rapidly declined again until 2020 (Fig. 5 *F* and *G*). Considering the whole time series, the lengths of industrial and domestic intermittent rivers decreased at rates of −4,917 km/y and −3,028 km/y (Fig. 5 *F* and *G*), driven primarily by the wetter conditions experienced throughout the whole time series. The decline in intermittent river lengths before 1970 was partly due to increased streamflow caused by the cooler climate (*SI Appendix*, Fig. S4). Then the length of intermittent rivers increased after 1972 due to rising water use by the domestic and industrial sectors as the socioeconomic situation improved. The length of agricultural intermittent rivers declined at a rate of −4,708 km/y (Fig. 5*E*), owing to waning irrigation demand and improved irrigation efficiency across China (22). At the basin scale, the length of sectoral functional intermittent rivers decreased most in the Northwest River drainage system, with decreases of −5,251 km/y, −5,347 km/y, and −5,667 km/y for the agricultural, domestic, and industrial sectors (Fig. 5*H* and *SI Appendix*, Fig. S9). Industrial and domestic intermittent river lengths increased significantly in most river basins, especially in the Liao, Hai, and Huai River basins during 1970–2010 (Fig. 5*H* and *SI Appendix*, Fig. S9).

## Discussion

Concepts such as flow connectivity and intermittency offer pathways by which to better understand river dynamics and, in turn, improve the management and safeguarding of rivers. We estimate that natural intermittent rivers, defined as rivers where streamflow ceased for at least one day per year on average during 1961–2020, occupy approximately 13% of all river reaches in mainland China. This proportion is a spatially explicit, highly credible estimate of nonperennial rivers under natural conditions across China, and aligns with previous studies. For example, Messager et al. (6) predicted the distribution of global intermittent rivers using first-order extrapolation from a random forest model and reported a 46% average probability of flow intermittence throughout China. Zhang et al. (30) identified about 17 of 45 intermittent stations (~38%) within the Huai River basin. The discrepancy in intermittent river proportions between the present and previous studies can be attributed to differences between approaches (for example, use of modeled, bias-corrected discharge instead of extrapolated, measured streamflow), the definition of river intermittency, and differences in resolution and quality of data across China.

Our study has provided evidence of a decline in natural intermittent rivers, as demonstrated by the decrease in nonperennial river length of −233 km/y across China from 1961 to 2020, and estimated the impacts of climate change and human water withdrawals on river intermittency. By conducting climate-detrending simulations and exploring changes in river intermittency for different levels of observed climate change, we found an offsetting effect of warming temperature on the decrease in natural intermittent river length in China. Anthropogenic forcing, dominated by greenhouse gas emissions, is the main driver of the observed warming climate (31). Previous studies have consistently projected significant increases in surface mean temperature (32), evapotranspiration (32), and frequency of extreme temperature events (33) across China under high level of greenhouse gas emissions based on the Coupled Model Intercomparison Project Phase 6 simulations. Thus, the potential risk of river intermittency may be exacerbated by larger evaporative demand induced by higher temperatures in the future warming climate. Although a slight compensatory effect of earlier snowmelt in maintaining natural streamflow was found to occur for high warming-wetting (Fig. 4),

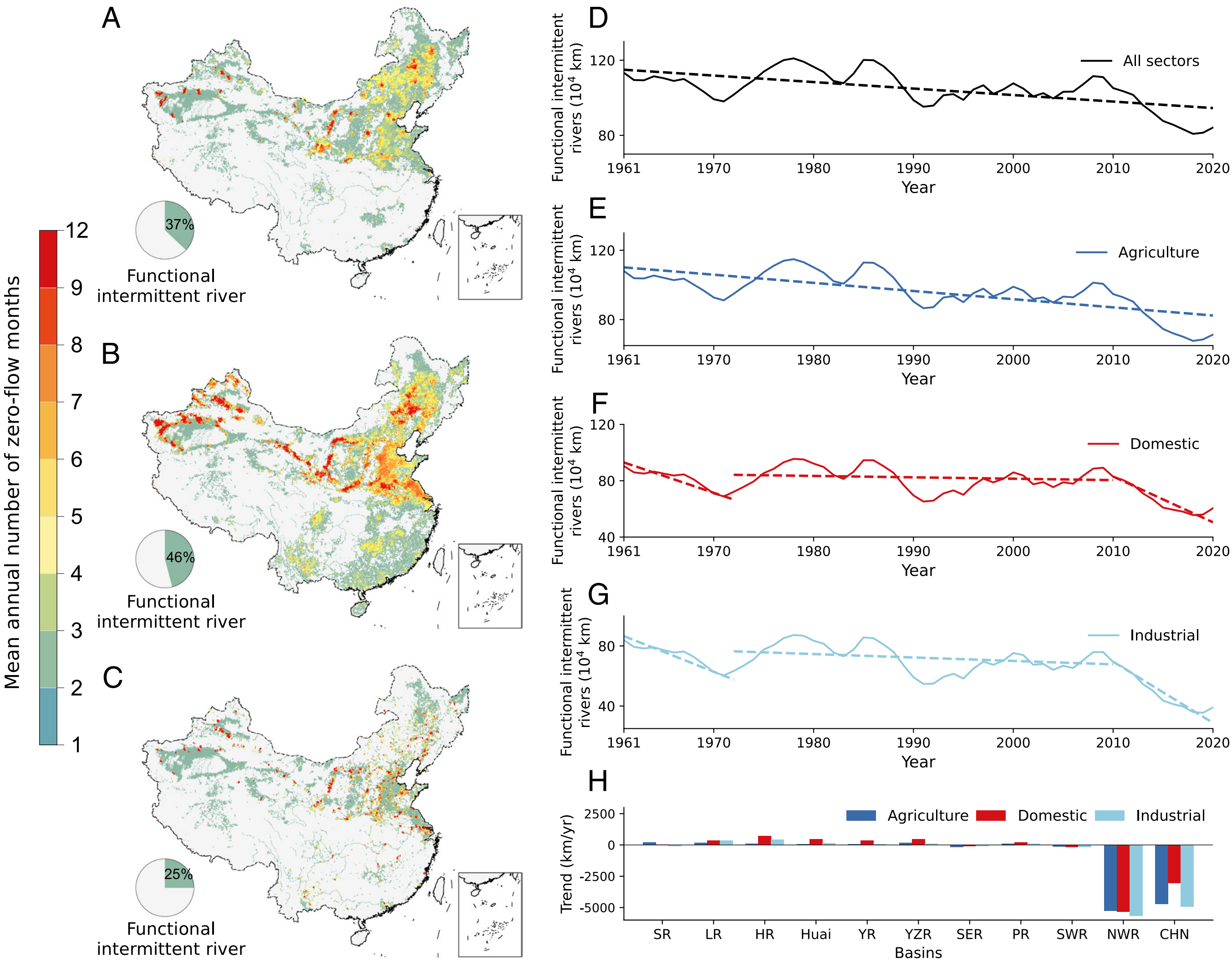


**Fig. 5.** Distribution and changes in river flow functional connectivity during 1961–2020 throughout China. (*A*–*C*) Spatial distribution of mean annual number of zero-flow months for 217,001 river reaches, after considering environmental streamflow and water withdrawal by the domestic, agricultural, and industrial sectors. Note that a zero-flow month means that the natural streamflow obtained by subtracting the water withdrawal volume of a given sector was unable to meet the monthly environmental flow requirements of a specific river reach (*Materials and Methods*). (*D*–*G*) Time series of annual functional intermittent river length in terms of different water withdrawal sources. Solid lines indicate the total annual intermittent river lengths induced by water withdrawal from all, agricultural, domestic, and industrial sectors. Dashed lines are fitted linear trend lines for the corresponding period. Note that intermittent rivers for the combined sectors were recalculated according to total water withdrawals. (*H*) Linear trends in the functional intermittent river lengths (km/y) due to water withdrawal in agricultural, domestic, and industrial sectors for the ten large river basins in China (CHN), comprising the Songhua River (SR), Liao River (LR), Hai River (HR), Yellow River (YR), Huai River (Huai), Yangtze River (YZR), Southeast River drainage system (SER), Pearl River (PR), Southwest River drainage system (SWR), and Northwest River drainage system (NWR).

attention should be paid to the possibility of earlier snowmelt in winter and spring seasons (34), which may cause an increase in irrigation demand that must be met by new alternative water supplies (35), thus exacerbating river intermittency.

By exploring the pattern of river flow functional connectivity, we investigated the sustainability of the riverine system in China in terms of recent socioeconomic development, and thus assessed how to achieve a balance between natural streamflow and socioeconomic water withdrawal. This represents an advance on previous work on river intermittency (6, 11, 12, 19) by explicitly including human water withdrawal and environmental flow requirements, and considering hydrological connectivity as indicative of river carrying capacity. Notably, intermittent rivers tripled in length from 13 to 50% (mostly located in low-order reaches) in China when considering environmental flow requirements and total human water withdrawal from riverine systems, demonstrating that human activity has had a profound effect on China's natural water resources and eco-environment systems. The agricultural sector, with total irrigation water withdrawal of 291 billion $m^3/y$ during 1965–2020 across China, has promoted the most severe functional river intermittency (46% of all rivers) driven by the need to meet the rising food demand of China's more affluent, growing population. Water withdrawal by the industrial and domestic sectors resulted in 25 and 37% functional intermittency of all rivers, with decreasing lengths of −4,917 km/y and −3,028 km/y during 1961–2020. We found river flow connectivity to be unevenly distributed between south and north China. The majority of basins in water deficit are located in northern China, whereas water surplus regions tend to be located in the southeast (Figs. 1 and 5). This uneven river flow connectivity, in addition to uneven water quality and water demand [as reported in previous studies (22, 36)] could further exacerbate water deficit in northern China due to increased sectoral water withdrawal from the more arid northern basins where water is already very limited. If northern basins are unable to obtain alternative sources of water (e.g. through water diversion and desalination of seawater) or properly regulate human water withdrawals (e.g. by limiting agricultural expansion, improving irrigation efficiency, and recycling used industrial water) in a warming climate, then available water resources and socioeconomic development could both be adversely affected. These findings have important implications for natural water resources sustainability and thereby regional water security.

It should be noted that the physical parameterization of snowmelt and groundwater dynamics is not fully understood (37). This points to a need for improved modeling of streamflow trends and variability, and reduction of simulation uncertainty, which may be achieved through multimodel ensembles or refined representation of land-atmosphere processes in general circulation models. Furthermore, the zero-flow day threshold and minimum environmental flow requirement were set according to previous studies (6, 16, 38, 39). These two thresholds affect the distribution of natural and functional intermittent rivers, introducing uncertainty into river streamflow simulation. For simplicity, the natural river conditions is taken as the flow benchmark; the present study does not consider human activities such as land-use and land-cover changes and reservoir construction. In practice, reservoir operation can have both positive and negative effects on river connectivity, depending on the hydrological regime and the environmental flow requirements. Land-use change (40) and hydropower operation (41) also alter flow patterns and increase pressure on rivers and their connectivity. We therefore recommend future studies be undertaken to evaluate potential threats to river flow connectivity arising from land-use change, construction and operation of hydropower schemes, sand excavation, land reclamation, and other human activities.

The proposed daily reach-level streamflow dataset presented herein has been designed to inform national biogeochemical modeling and riverine species distribution models. The developed UDSBC bias-correction algorithm (freely available at https://github.com/jiaojiaogou/UDSBC) is directly applicable to other regions for land-surface modeling at national or basin scales. We hope this work can ultimately assist in explaining the patterns and driving mechanisms behind river flow connectivity help safeguard the integrity of river networks and hence maintain ecosystem stability.

## Materials and Methods

**Definition of Terms.**

***Natural streamflow.*** Streamflow data without interference from human activities.

***River flow connectivity.*** A river reach is considered disconnected (nonperennial) if its streamflow ceases for at least one day per year (determined as an interannual average over the 1961–2020 record).

***River flow functional connectivity.*** A river reach is considered functionally disconnected (nonperennial) if its streamflow does not meet water withdrawal volume and environmental flow requirements, such that the river was unable to provide societal, economic, and ecological services for at least one month per year on average during 1961–2020.

**Data Sources.**

***Hydrographic framework.*** The global vector-based river network dataset, MERIT-Basin (Multi-Error-Removed-Improved-Terrain-Basin) (42, 43), was adopted in our modeling framework. MERIT-Basin is a high-quality hydrographic mapping product that provides high-resolution river and catchment information. We extracted the nationwide river network, comprising 217,001 individual river reaches (i.e., line segments between confluences) across China, each of average length 8.7 km (SD = 8.6 km), covering a total of about $18.6 \times 10^5$ km of the river network available from the global MERIT-Basin hydrography database. Input to the routing model comprised spatial units of subcatchments and river centerlines, and the properties of each river reach (including catchment area, Strahler stream order level 1 to 8, channel length, and upstream/downstream links). Each river reach was linked to a polygon fitted to its contributing hydrological subcatchment, of average area about 43 $km^2$. Each "river reach" was defined as a basin outlet, thus representing the aggregation of upstream river reaches as a contiguous flow path from the headwater source to the outlet.

***Streamflow Data.*** High-density natural or near-natural streamflow records at 651 hydrological stations in the ten large river basins in mainland China were used to validate and revise the land surface model biases (*SI Appendix*, Fig. S10 and Note 1). *SI Appendix*, Table S1 lists summary information on the ten large river basins. Data from 651 hydrological stations, including 342 daily hydrological stations (2,166,938 d) and 309 monthly hydrological stations (79,379 mo) during 1961–1979, were obtained from the hydrological yearbook of China and local water resources departments (*SI Appendix*, Fig. S10 *A* and *B*). These datasets included both naturalized and observed streamflow value. Note that nearly half of all gauge records were naturalized by the Ministry of Water Resources of China based on the water balance principle (*SI Appendix*, Note 1). The naturalization procedure involved removal of major flow alterations caused by human activities, such as agricultural irrigation, industrial consumption, domestic consumption, water diversion, and reservoir storage (23). The remaining gauge records were all near-natural with no upstream dams present and a low level of human interference during the selected near-natural research period (noting the boom in socioeconomic activity in China after 1980). Drainage areas for the 651-gauge catchments ranged from 17.5 to 1,705,383 $km^2$, with a total drainage area of $45.9 \times 10^5$ $km^2$, or about 62.4% of the nonice, nondesert land area of China.

***Climatic Data.*** Meteorological forcing variables included daily precipitation, maximum temperature, minimum temperature, and wind speed. To drive the land-surface models and separate the historical climatic change regions, we used observed climate data from the China Meteorological Administration (CMA) and China Hydro-Meteorology datasets (CHM) (44, 45) over the study period from 1961 to 2020 inclusive. The 0.1° × 0.1° gridded meteorological forcing data (CHM_pre and CHM_temp) were previously interpolated from the CMA using data from ~2,400 gauge stations. This spatial resolution is consistent with the average length of the river reaches (8.7 km) and minimizes the impact of scale mismatch. CHM_pre comprised daily gridded precipitation data (44), available at 0.1° × 0.1° grid resolution for 1961 to 2020, and were generated from in-situ gauge data using an optimal interpolation method (i.e., by combining the daily climatology field with a precipitation ratio field using inverse-distance weighting). CHM_temp comprised daily 0.1° × 0.1° gridded temperature data, generated from in-situ gauge data by combining climatology and anomaly fields using angular-distance weighting. Other climate forcing variables, such as downward shortwave radiation, longwave radiation, vapor pressure, and air pressure were simulated offline by the Mountain Climate Simulator (https://github.com/jhamman/mtclim5). Daily precipitation and mean temperature were also used to determine historical climate conditions for each river reach.

***Human water withdrawal.*** We created a long-term national sectoral water withdrawal and groundwater withdrawal dataset at 0.1° × 0.1° spatial resolution and monthly time interval using water use data reported by Huang et al. (46, 47) and several spatial-temporal statistical downscaling algorithms for 1965–2020 (*SI Appendix*, Fig. S11). The developed dataset was aggregated into three water-use sectors: agricultural (irrigation), domestic, and industrial (electricity generation, manufacturing, and mining). Huang et al.'s water-use data were developed from survey-based water withdrawal and water availability datasets, including the National Long-term Water Use Dataset of China (see ref. 22) and water-use statistics reported in the China Water Resources Bulletin. Further details about the water withdrawal dataset are given by Huang et al. (46). Huang et al.'s water use data are only available at 0.25° × 0.25° grid resolution at an annual scale during 1965 to 2020; thus, we downscaled the data spatiotemporally to match our model domain. For industrial water withdrawal, we spatiotemporally downscaled water-use data using the 0.1° × 0.1° high-resolution monthly industrial water withdrawal mapping provided by Hou et al. (48), based on about 400,000 records of industrial enterprises, and monthly industrial product output data across China. For agriculture water withdrawal, we adopted the global irrigated cropland area map for the year 2000 from the Global Map of Irrigation Areas version 5 (49) as the spatial field for spatial downscaling. The global population density map for the year 2000 in the Socioeconomic Data and Application Center was utilized in spatial downscaling of water withdrawal records for the domestic sector and groundwater withdrawal. Previous global monthly water withdrawal datasets from Huang et al. (20) were used for temporal downscaling of agriculture and domestic water withdrawal. Water consumption volumes were reconstructed based on aggregated return flow ratio data extracted from the China Water Resources Bulletin at the basin level by Huang et al. (46).

**Land Surface Modeling and Bias Correction.**

***Land surface model.*** The Variable Infiltration Capacity land surface model version 5 (VIC-5) was used to reconstruct historical natural runoff records (50, 51). This VIC model simulates surface and subsurface hydrologic processes at spatially distributed grid cells, as well as water fluxes into and out of three soil layers. By exploiting parallelization, VIC-5 is computationally efficient and therefore suitable for large-scale high-resolution simulations. In this study, we ran the VIC-5 model in water balance mode for China with a daily time step. Well-trained VIC model parameter sets had been previously estimated (15, 23) within a comprehensive parameter uncertainty analysis framework. Following sensitivity analysis results, we optimized the model parameters automatically against naturalized streamflow records and estimated regional-scale model parameters for ungauged catchments with fine soil texture properties. Daily time series of grid-level (0.1° × 0.1°) natural runoff for 1961–2020 were reconstructed to assess the distribution and variability of river flow connectivity throughout China. The 1 km 1992–1993 global land cover dataset from the University of Maryland and downscaled monthly 0.1° × 0.1° global leaf area index database for 1981–1993 supplied by Myneni et al. (52) were used to generate the 0.1° × 0.1° subvegetation parameter distribution for the model. Note that the subvegetation parameter remained unchanged in the simulation framework to avoid human interference affecting the long-term natural streamflow simulation. Details of the model parameter calibration procedure and other input datasets (e.g., soil, and topographical data) are given in refs. 15, 23, 53.

***River routing model.*** The Routing Application for Parallel Computation of Discharge (RAPID) model (54) was used to calculate river-reach-level routing discharge through a dendritic river network. In RAPID, river channel routing is performed using a vector-based river network, with a matrix form of the Muskingum equation solved using a highly efficient linear system solver. The RAPID model was forced by previously constructed daily lateral inflows during 1961–2020 obtained from variable infiltration capacity (VIC) runoff data across mainland China. Two model parameters, the flood wave travel parameter $k$ and the dimensionless weighting factor $x$, were estimated for each vector river flowline, as described by Lin et al. (42). For each river reach, an estimate of the mean long-term (1961–2020) lateral inflow was derived through an area-weighted mapping technique (42, 55) from the 0.1° × 0.1° gridded runoff dataset. (Area weighted information was computed using scripts available from https://github.com/peironglinlin/GlobalHydro/.)

***Bias correction.*** In support of the optimization framework, we examined the performance of 651 gauge stations. To limit model uncertainty as much as possible, a statistical postprocessing procedure named "Upstream-Downstream Scaled Bias Correction" (UDSBC, https://github.com/jiaojiaogou/UDSBC) was developed for daily streamflow bias correction of each river reach based on the Scaled Distribution Mapping technique (56). *SI Appendix*, Note 2 provides details of the UDSBC method. *SI Appendix*, Note 3 describes the four skill metrics, LogCC, LogNSE, Pbias, and LogKGE, used to evaluate the performance of the reconstructed streamflow data. The log transform version of metrics placed greater weight on low-flow days of interest for intermittence. The results confirmed that the calibrated VIC model provided reliable lateral inflows for the RAPID model, with 71% and 75% of the daily and monthly stations having Kling–Gupta efficiency in logarithmic space (LogKGE) > 0.6, respectively (*SI Appendix*, Fig. S10 *C* and *D*).

***Validation.*** *SI Appendix*, Fig. S12 presents validation results for daily streamflow reconstruction performance at 342 hydrological stations during 1961–1979. The results show that the bias-corrected daily streamflow closely matches observations, with a median LogNSE of 0.54 and median LogKGE of 0.75. Notably, LogNSE and LogKGE exceeds 0 for 85% and 97% of the daily streamflow stations, confirming that our hydrological models and postprocessing bias-correction algorithm provided a robust framework by which to quantify the intermittency of rivers in China. We also evaluated the ability of the reconstructed streamflow to identify the state of river flow intermittence (provided the streamflow ceased for at least one day per year over the period 1961–1979) by comparing the average number of zero-flow days obtained for simulated and observed discharges. The result confirmed that the reconstructed runoff accurately captured river connectivity status with an accuracy rate of 77% among 342 daily stations. These foregoing results indicate that the reconstructed river streamflow is generally capable of capturing observed flow regimes and can thus be used to analyze river flow connectivity at the river-reach level.

**River Flow Connectivity Signatures.** Three temporal streamflow signatures, which quantify the natural river flow connectivity status of individual reaches (*SI Appendix*, Fig. S13), were given by the number of zero-flow days (streamflow <0.001 $m^3/s$), the number of zero-flow periods (average number of consecutive zero-flow events), and the duration of zero-flow periods (average duration of consecutive zero-flow events). Each streamflow signature was calculated on an annual basis from bias-corrected streamflow data. We first calculated the number of zero-flow days in each year for each reach and then calculated the annual average number of zero-flow days over the study period for each reach. We considered a river reach to be intermittent if its stream ceased to flow for at least one day per year on average during the 1961–2020 record. This definition of river flow connectivity is supported by previous research on flow regimes worldwide (6, 16). The flow threshold of zero-flow days was set at 0.001 $m^3/s$ to avoid potential false positive detection of zero flows associated with modeling structure constraints and uncertainty in streamflow simulation. A simplified dendritic connectivity index (DCI, ranging from 0 to 100%) was used to evaluate the spatial connectivity of each large river basin considered and quantified in terms of the length of zero-flow reach fragments. *SI Appendix*, Note 4 provides details of the calculation of the DCI. Following Jaeger et al. (5), we considered a reach to be any continuous segment of adjacent reaches (with river network topology connection) carrying nonzero flow (a spatially continuous wet reach) and evaluated DCI values, summing over all possible pairs of wet reaches, for each day of model output. The index was scaled from 0 (low spatial connectivity) to 100% (high spatial connectivity).

**Climate Change Impact Analysis.** Observed linear trends of temperature and precipitation were determined using the linear least-squares regression method at the river reach level. We first downscaled the climate variables from the 0.1° × 0.1° grid to subcatchment scale (with a mean drainage area of 43 $km^2$) using the area-weighted mapping technique (44, 55). Then we searched the upstream rivers and calculated the basin average of climate variables for each river reach on each day during 1961 to 2020. We focused solely on warming climate change in the historical climatology because most of the river catchments experienced positive temperature change (~99%, *SI Appendix*, Fig. S3*D*), reflective of the warming climate (17). The intersection between the observed rates of change in each climate variable (across all locations) and corresponding $P$-value of 0.05 (Mann–Kendall test) was used to identify whether a given river reach had experienced a significant change in the climate variable. Warming levels were derived according to the probability density distribution of temperature change rate: with high (>75th percentile), moderate (between 25th and 75th percentiles), and low warming (between the 0.05 significant change threshold and 25th percentile). Hence, we divided China's river reaches into six regions based on observed annual temperature and precipitation rates of change over the period 1961–2020 (*SI Appendix*, Fig. S14).

To examine climate change impact on river intermittency, we used linear detrending methods for the climate forcing in the VIC5 model. Linear detrending involved removing the gradients of annual temperature and precipitation between 1961 and 2020. Modeled annual intermittent river lengths were compared between the raw forcing simulation (S1), the temperature-detrended forcing simulation (S2), and the precipitation-detrended forcing simulation (S3). Note that the S2 and S3 streamflows included UDSBC bias correction while preserving simulated changes (*SI Appendix*, Note 2). We used hypothesis testing to evaluate the significance of our results. Student's $t$-tests were used to compare the difference in intermittent river length between the two simulation results. The SciPy library in Python was used to implement the $t$-test based on the $t$-distribution for CI and $P$-values. To further explore the role of climate change, we analyzed changes in river flow connectivity signatures (zero-days, zero-flow periods, and zero-flow period durations) for the six climate change regions of interest, which involved three warming-wetting trends, $T_LP_+$, $T_MP_+$, $T_HP_+$, and three warming-drying trends, $T_LP_-$, $T_MP_-$, $T_HP_-$ (*SI Appendix*, Fig. S14). We then extracted annual climate and river intermittency signatures for wet (May-October) and dry (November-April) seasons. We assumed a half-year period during which the maximum (minimum) of available water occurred in the wet (dry) season using the same criteria for each year throughout 1961 to 2020. We estimated river flow connectivity changes for both the wet and dry seasons from the linear trends in the three river temporal connectivity signatures for each climate change region.

**Human Water Withdrawal Impact Analysis.** To explore the need or potential of river bearing capacity, we assumed the environmental streamflow to be the threshold at which river flow functional connectivity occurs. In other words, we examined whether the flow volume in a river reach minus sectoral water withdrawal (46) demand could meet the requirement for ecological sustainability. In the present study, environmental flow refers to the potential surface water streamflow volume required to sustain the aquatic ecosystem and its surrounding environment. Following Rodrigues et al. (38) and Wada et al. (39), we considered Q90, i.e., the daily streamflow that was exceeded 90% of the time during the research period (1961–2020), as the minimum environmental flow requirement for each river reach. We applied the area-weighted average approach (*SI Appendix*, Note 5) to estimate the river-reach-level water withdrawal and then aggregated the values for each individual river by accumulating estimates for the upstream reaches, based on the developed 0.1° × 0.1° gridded withdrawal yield values for each of the three sectors. Using modeled and bias-corrected monthly streamflow values, we calculated the average number of functional connectivity months per year, based on mean water withdrawal during the corresponding decadal phase and Q90 values for each river reach. Note that the functional connectivity months during 1961–1964 were calculated by subtracting the water withdrawal volumes from 1965. We considered a river reach to be ineffective in terms of functional connectivity in cases where the stream ceased to flow for at least one month per year on average during the 1961–2020 record.

**Data, Materials, and Software Availability.** MERIT-Basin hydrography products have been deposited in Google Drive (https://www.reachhydro.org/home/params/merit-basins) (43); sectoral human water withdrawal datasets data have been deposited in Zenodo (https://doi.org/10.5281/zenodo.7849026) (47). All study data are included in the article and/or *SI Appendix*.

**ACKNOWLEDGMENTS.** This work was supported by the National Natural Science Foundation of China (U24A20572, 42401016), the 111 Project of China (B23027), and Fundamental Research Funds for the Central Universities. L.S. is funded through UKRI (MR/V022008/1). We are grateful to the Center for Geodata and Analysis, Faculty of Geographical Science, Beijing Normal University (https://gda.bnu.edu.cn/), for its high-performance computing support.

Author affiliations: [a]State Key Laboratory of Earth Surface Processes and Disaster Risk Reduction, Faculty of Geographical Science, Beijing Normal University, Beijing 100875, China; [b]Department of Geographic Science, Faculty of Arts and Sciences, Beijing Normal University, Zhuhai 519087, China; [c]Key Laboratory of Water and Sediment Sciences, Ministry of Education, College of Environmental Sciences and Engineering, Peking University, Beijing 100871, China; [d]Department of Civil and Environmental Engineering, University of California, Irvine, CA 92697; [e]College of Hydrology and Water Resources, Hohai University, Nanjing 210098, China; [f]State Key Laboratory of Simulation and Regulation of Water cycle in River Basin, China Institute of Water Resources and Hydropower Research, Beijing 100038, China; [g]School of Geography and the Environment, University of Oxford, Oxford OX1 3QY, United Kingdom; [h]College of Water Sciences, Beijing Normal University, Beijing 100875, China; [i]Beijing Key Laboratory of Urban Hydrological Cycle and Sponge City Technology, Beijing, 100875, China; [j]School of Engineering, The University of Edinburgh, Edinburgh EH9 3JL, United Kingdom; [k]School of Engineering, Computing and Mathematics, University of Plymouth, Plymouth PL4 8AA, United Kingdom; [l]Department of Geography, University of California, Los Angeles, CA 90095; and [m]Biological and Environmental Science and Engineering Division, King Abdullah University of Science and Technology, Thuwal 23955, Saudi Arabia

1. G. Grill *et al.*, Mapping the world's free-flowing rivers. *Nature.* **569**, 215–221 (2019).
2. X. Wang *et al.*, Gainers and losers of surface and terrestrial water resources in China during 1989–2016. *Nat. Commun.* **11**, 3471 (2020).
3. Y. Wang *et al.*, Sustainability of global golden inland waterways. *Nat. Commun.* **11**, 1553 (2020).
4. D. A. Edmonds, R. L. Caldwell, E. S. Brondizio, S. M. O. Siani, Coastal flooding will disproportionately impact people on river deltas. *Nat. Commun.* **11**, 4741 (2020).
5. K. L. Jaeger, J. D. Olden, N. A. Pelland, Climate change poised to threaten hydrologic connectivity and endemic fishes in dryland streams. *Proc. Natl. Acad. Sci. U.S.A.* **111**, 13894 (2014).
6. M. L. Messager *et al.*, Global prevalence of non-perennial rivers and streams. *Nature.* **594**, 391–397 (2021).
7. D. C. Allen *et al.*, River ecosystem conceptual models and non-perennial rivers: A critical review. *Wires Water* **7**, e1473 (2020).
8. E. Sauquet *et al.*, Classification and trends in intermittent river flow regimes in Australia, northwestern Europe and USA: A global perspective. *J. Hydrol.* **597**, 126170 (2021).
9. X. Shao, Y. Fang, B. Cui, A model to evaluate spatiotemporal variations of hydrological connectivity on a basin-scale complex river network with intensive human activity. *Sci. Total Environ.* **723**, 138051 (2020).
10. Q. Zhang *et al.*, Evaluation of ecological instream flow considering hydrological alterations in the Yellow River basin, China. *Glob Planet Change.* **160**, 61–74 (2020).
11. T. H. Snelder *et al.*, Regionalization of patterns of flow intermittence from gauging station records. *Hydrol. Earth Syst. Sci.* **17**, 2685–2699 (2013).
12. S. C. Zipper *et al.*, Pervasive changes in stream intermittency across the United States. *Environ. Res. Lett.* **16**, 084033 (2021).
13. T. Datry *et al.*, Flow intermittence and ecosystem services in rivers of the anthropocene. *J. Appl. Ecol.* **55**, 353–364 (2020).
14. J. P. Benstead, D. S. Leigh, An expanded role for river networks. *Nat. Geosci.* **5**, 678–679 (2012).
15. J. J. Gou *et al.*, CNRD v1.0: A high-quality natural runoff dataset for hydrological and climate studies in China. *Bull Am Meteorol Soc.* **102**, E929–E947 (2021).
16. D. Feng *et al.*, Recent changes to Arctic river discharge. *Nat. Commun.* **12**, 6917 (2021).
17. V. Masson Delmotte, *et al.*, Eds., *IPCC Climate Change 2021: The Physical Science Basis. Contribution of Working Group I to the Sixth Assessment Report of the Intergovernmental Panel on Climate Change* (Cambridge Univ. Press, 2021).
18. D. Šarauskienė *et al.*, Impact of physico-geographical factors and climate variability on flow intermittency in the rivers of water surplus zone. *Hydrol Process.* **34**, 4727–4739 (2020).
19. L. V. Reynolds, P. B. Shafroth, N. LeRoy Poff, Modeled intermittency risk for small streams in the Upper Colorado River Basin under climate change. *J. Hydrol.* **523**, 768–780 (2015).
20. Z. Huang *et al.*, Reconstruction of global gridded monthly sectoral water withdrawals for 1971–2010 and analysis of their spatiotemporal patterns. *Hydrol. Earth Syst. Sci.* **22**, 2117–2133 (2018).
21. P. Döll, K. Fiedler, J. Zhang, Global-scale analysis of river flow alterations due to water withdrawals and reservoirs. *Hydrol. Earth Syst. Sci.* **13**, 2413 (2009).
22. F. Zhou *et al.*, Deceleration of China's human water use and its key drivers. *Proc. Natl. Acad. Sci. U.S.A.* **117**, 7702–7711 (2020).
23. C. Miao *et al.*, High-quality reconstruction of China's natural streamflow. *Sci. Bull.* **67**, 547–556 (2022).
24. D. Cote, D. G. Kehler, C. Bourne, Y. F. Wiersma, A new measure of longitudinal connectivity for stream networks. *Landsc. Ecol.* **24**, 101–113 (2008).
25. Y. Sun *et al.*, Contribution of urbanization to warming in China. *Nat. Clim. Chang.* **6**, 706–709 (2016).
26. D. Li *et al.*, Exceptional increases in fluvial sediment fluxes in a warmer and wetter High Mountain Asia. *Science.* **374**, 599–603 (2021).
27. R. S. Padrón *et al.*, Observed changes in dry-season water availability attributed to human-induced climate change. *Nat. Geosci.* **13**, 477–481 (2020).
28. B. Udall, J. Overpeck, The twenty-first century Colorado River hot drought and implications for the future. *Water Resour. Res.* **53**, 2404–2418 (2017).
29. Z. Ban *et al.*, Understanding the asymmetry of annual streamflow responses to seasonal warming in the western U.S.. *Water Resour. Res.* **56**, e2020WR027158 (2020).
30. Y. Zhang *et al.*, Classification of flow regimes for environmental flow assessment in regulated rivers: The Huai River Basin. China. *River Res. Appl.* **28**, 989–1005 (2012).
31. Y. Sun *et al.*, Understanding human influence on climate change in China. *Natl. Sci. Rev.* **9**, nwab113 (2022).
32. Q. You *et al.*, Temperature dataset of CMIP6 models over China: Evaluation, trend and uncertainty. *Clim. Dyn.* **57**, 17–35 (2021).
33. H. Zhu, Z. Jiang, L. Li, Projection of climate extremes in China, an incremental exercise from CMIP5 to CMIP6. *Sci. Bull.* **66**, 2528–2537 (2021).
34. M. Xiao, A warning of earlier snowmelt. *Nat. Clim. Chang.* **11**, 380–381 (2021).
35. Y. Qin *et al.*, Agricultural risks from changing snowmelt. *Nat. Clim. Chang.* **10**, 459–465 (2020).
36. T. Ma *et al.*, Pollution exacerbates China's water scarcity and its regional inequality. *Nat. Commun.* **11**, 650 (2020).
37. M. Pan *et al.*, Snow process modeling in the North American Land Data Assimilation System (NLDAS): 2. Evaluation of model simulated snow water equivalent. *J. Geophys. Res. Atmos.* **108**, 1–11 (2003).
38. D. B. B. Rodrigues, H. V. Gupta, E. M. Mendiondo, P. T. S. Oliveira, Assessing uncertainties in surface water security: An empirical multimodel approach. *Water Resour. Res.* **51**, 9013–9028 (2015).
39. Y. Wada, M. F. P. Bierkens, Sustainability of global water use: Past reconstruction and future projections. *Environ. Res. Lett.* **9**, 104003 (2014).
40. V. B. Chagas, P. L. Chaffe, G. Blöschl, Climate and land management accelerate the Brazilian water cycle. *Nat. Commun.* **13**, 5136 (2022).
41. G. Di Baldassarre *et al.*, Water shortages worsened by reservoir effects. *Nat. Sustain.* **1**, 617–622 (2018).
42. P. R. Lin *et al.*, Global reconstruction of naturalized river flows at 2.94 million reaches. *Water Resour. Res.* **55**, 6499–6516 (2019).
43. P. Lin *et al.*, MERIT-Basins hydrography (based on MERIT-Hydro v0.7/v1.0). Google Drive. https://drive.google.com/drive/folders/1uCQFmdxFbjwoT9OYJxw-pXaP8q_GYH1a. Deposited 20 April 2023.
44. J. L. Hu *et al.*, An upgraded high-precision gridded precipitation dataset for the Chinese mainland considering spatial autocorrelation and covariates. *Earth Syst. Sci. Data Discuss.* (2025), 10.5194/essd-2025-20.
45. Q. Zhang *et al.*, A new high-resolution multi-drought-index dataset for mainland China. *Earth Syst. Sci. Data* **17**, 837–853 (2025).
46. Z. Huang *et al.*, Groundwater depletion rate over China during 1965–2016: The long-term trend and inter-annual variation. *J. Geophys. Res. Atmos.* **128**, e2022JD038109 (2023).
47. Z. W. Huang *et al*., Supplementary data for "Groundwater depletion rate over China during 1965-2016: the long-term trend and inter-annual variation." Zenodo. https://doi.org/10.5281/zenodo.7849026. Deposited 19 March 2019.
48. C. C. Hou *et al.*, High-resolution mapping of monthly industrial water withdrawal in China from 1965 to 2020. *Earth Syst. Sci. Data* **16**, 2449–2464 (2024).
49. S. Siebert, V. Henrich, K. Frenken, J. Burke, "Global map of irrigation areas version" in *Rheinische Friedrich-Wilhelms-University, Bonn, Germany/Food and Agriculture Organization of the United Nations, Rome, Italy* (2013), **vol. 5**, pp. 1299–1327.
50. X. Liang, D. P. Lettenmaier, E. F. Wood, S. J. Burges, A simple hydrologically based model of land surface water and energy fluxes for general circulation models. *J. Geophys. Res. Atmos.* **99**, 14415–14428 (1994).
51. J. J. Hamman *et al.*, The variable infiltration capacity model version 5 (VIC-5): Infrastructure improvements for new applications and reproducibility. *Geosci. Model Dev.* **11**, 3481–3496 (2018).

52. R. B. Myneni *et al*. Estimation of global leaf area index and absorbed PAR using radiative transfer models. *IEEE Trans. Geosci. Rem. Sens.*, **35**, 1380–1393 (1997).
53. J. J. Gou *et al.*, Sensitivity analysis-based automatic parameter calibration of the variable infiltration capacity (VIC) model for streamflow simulations over China. *Water Resour. Res.* **56**, e2019WR025968 (2020).
54. C. H. David *et al.*, River network routing on the NHDPlus dataset. *J. Hydrometeorol.* **12**, 913–934 (2011).
55. P. Lin *et al.*, Implementation of a vector-based river network routing scheme in the community WRF-Hydro modeling framework for flood discharge simulation. *Environ. Model. Softw.* **107**, 1–11 (2020).
56. M. B. Switanek *et al.* Scaled distribution mapping: a bias correction method that preserves raw climate model projected changes. *Hydrol Earth Syst Sc*. **21**, 2649–2666 (2017).